Final Draft
of the original manuscript:

Fronczek, D.M.; Chulist, R.; Litynska-Dobrzynska, L.; Kac, S.; Schell, N.; Kania, Z.; Szulc, Z.; Wojewoda-Budka, J.:

Microstructure and kinetics of intermetallic phase growth of three-layered A1050/AZ31/A1050 clads prepared by explosive welding combined with subsequent annealing

In: Materials and Design (2017) Elsevier

DOI: 10.1016/j.matdes.2017.05.051

Microstructure and kinetics of intermetallic phase growth of three-layered A1050/AZ31/A1050 clads prepared by explosive welding combined with subsequent annealing

D.M. Fronczek[a,*], R. Chulist[a], L. Litynska-Dobrzynska[a], S. Kac[b], N. Schell[c], Z. Kania[a], Z. Szulc[d], J. Wojewoda-Budka[a]

[a]Institute of Metallurgy and Materials Science Polish Academy of Sciences, 25 Reymonta Street; 30-059 Cracow; Poland
[b]AGH University of Sciences and Technology, 30 Mickiewicza Ave. 30-059 Cracow, Poland
[c]Institute of Materials Research, Helmholtz-Zentrum Geesthacht, Max-Planck-Strasse 1, D-21502 Geesthacht, Germany
[d]High Energy Technologies Works 'Explomet', 100H Oswiecimska Street; 45-641 Opole; Poland

[*] Corresponding author: d.fronczek@imim.pl; +48122952889
r.chulist@imim.pl; l.litynska@imim.pl; slawomir.kac@agh.edu.pl; norbert.schell@hzg.de; z.kania@imim.pl; zszulc@op.onet.pl; j.wojewoda@imim.pl

Abstract
The effect of annealing has been investigated with respect to interface microstructure and evolution of intermetallic phases in three-layered explosively welded A1050/AZ31/A1050 specimens. Both interfaces in the state after welding were characterized by wavy shape morphology with intermediate phases, which formed segmented structures. Two different morphologies consisted of equiaxed and columnar grains were observed within the Mg_2Al_3 phase, while the $Mg_{17}Al_{12}$ phase was built of columnar grains only. Furthermore, a small amount of $Mg_{23}Al_{30}$ was detected by X-ray synchrotron diffraction. Annealing at 350 °C strongly induced the $Mg_{23}Al_{30}$ phase development in the form of discontinuous layer between Mg_2Al_3 and $Mg_{17}Al_{12}$ phases after 10 h of annealing. Kinetics calculations indicated that, Mg_2Al_3 phase growth at 300 °C was controlled by different mechanisms according to the location: volume diffusion and chemical reaction at the upper interface and solely by volume diffusion at lower one. The growth of $Mg_{17}Al_{12}$ was governed only by volume diffusion. Furthermore, the same mechanisms were observed during annealing at 400 °C, however this heat treatment significantly changed the microstructure i.e. the grain size and shape. It was also established that the nanohardness of both Mg_2Al_3 and $Mg_{17}Al_{12}$ was about 350 HV.

Keywords: explosive welding; interface; intermetallic phases; magnesium; aluminum;

1. Introduction

Magnesium alloys apart from such advantages as good machinability and thermal conductivity exhibit electromagnetic interference shielding as well as vibration absorption. These features combined with corrosion resistance and high strength to weight ratio of aluminum alloys placed on the both side of magnesium alloy may be interesting solution for ballistic shield production. On the other hand, the explosive welding technology of very thin layers is very challenging and therefore expensive. One of the ways to overcome this problem is to combine the explosive welding with rolling to obtain the high-strength joint with very thin interlayers. This in turn indicates the issue of intermetallic phase presence at the interface of joined materials.

A number of numerical simulations and experiments have been performed in order to design light materials of good strength and high resistance to corrosion suitable for the defense industry [1-4]. Obtaining a continuous intermetallic layer in-between light metals is highly desirable. Rohatgi et al. [5], Konieczny et al. [6] or Thiyaneshwaran et al. [7] reported that multi-layered sandwiches formed from the monomers of Ti-$TiAl_3$ intermetallic phase [5], Ni-($NiAl_3$+Ni_2Al_3) and Ni-Ni_2Al_3 [6] or Ti-$TiAl_3$ intermetallic phase - Al [7] were characterized by a significant improvement of mechanical properties. Therefore, many techniques such as forging [8], insert molding [9], pressing [10], and rolling [11] usually combined with heat treatment were applied to obtain good quality of joints with hard intermetallics in-between. Due to its simplicity and economic reasons, explosive welding (EXW) was also used in joining of Mg and Al alloys [12-20].

EXW is classified as a cold solid-state process, in which no heat affected zone is detected [21,22]. Moreover, due to the presence of the jet, self-cleaning of joined surfaces can be noticed and both oxides and impurities after being stripped away are no longer present at the bonded area [23,24]. However, despite these advantages, the studies on magnesium/aluminum composites manufactured by EXW are still scarce and come down to the investigation of only two-layer materials.

The first attempts to obtain the Mg/Al composite described in work of Trykov et al. [12] in 2003 considered four materials: magnesium alloy (MA2-1), titanium alloy (VT1-0) and two various aluminum alloys (AD1 and AMg6). However, the applied magnesium alloy sample was not situated in the direct contact with the aluminum alloy. Therefore, the Mg/Al interface could not be investigated. The tests, which resulted in manufacturing the direct Mg/Al bond were described in two papers [13,14]. No intermediate phases were observed at the interface in the state directly after EXW, while the application of annealing led to obtaining three intermetallics, namely Al_3Mg_2, $Al_{12}Mg_{17}$, Al_2Mg_3, confirmed by the X-ray diffraction (XRD) measurements. Those microstructural observations were also supplemented with hardness and microhardness measurements [13,14].

The influence of the heat treatment on explosively welded two-layered Mg/Al was investigated in work of Zhang et al. [15]. It was demonstrated that the formation of Al_3Mg_2 on the Al side and $Al_{12}Mg_{17}$ on the Mg side took place during annealing at above 252 °C for 2 h. However, the microstructure of interface region and the phase composition was described solely by means of scanning electron microscopy with energy-dispersive X-ray spectroscopy (SEM/EDS) with the support of mechanical tests [15]. A comprehensive description and understanding of the phenomena occurring within the explosively welded materials can be carried out only by the examination of the microstructure at different scales and using supplementary techniques [25-27].

A different description of the Al and Mg interface region after EXW was given in work of Ghaderi et al. [16], where the $MgAl_2$ intermediate phase forming swirls, was locally and randomly distributed at the interface. Its presence was confirmed by both SEM/EDS and XRD measurements. However, the state after annealing was not examined.

In other reports dealing with the explosively welded Mg/Al, despite the application of various techniques such as transmission electron microscope or synchrotron measurements, no intermetallic phases were detected [17-19]. A numerical calculation concerning the EXW process of Mg/Al composites was given in work of Yuan et al. [20].

The explosively welded A1050/AZ31/A1050 clads investigated in the paper were rolled in order to obtain a thin Mg alloy interlayer. The goal of the study was to investigate the resulting microstructure and its development during the annealing process. Such an examination could confirm or exclude the proposed experiment for further technological studies. Therefore, the complex analysis of material response to EXW followed by rolling combined with further thermal treatment at the macro-, micro- and nanoscale of three-layered

A1050/AZ31/A1050 clads was performed. It mainly included the investigation of relation between the interface area and the explosive material, with the particular attention to the intermetallic phases occurring under harsh conditions of extremely high pressure and rapid crystallization. A detailed analysis of the heat treatment influence on the intermetallics development and the growth kinetics of intermediate phase calculations was given coupled with the microstructure description based on SEM, transmission electron microscopy (TEM) and electron backscattered diffraction (EBSD) observations. The electron microscopy techniques allow examining the chemical composition changes, grain size, shape, and orientations in the joined materials in regions adjacent to the interface. Finally the microstructure changes were related to hardness and nanohardness tests.

2. Materials and methods

Two plates of A1050 aluminum alloy and one of AZ31 magnesium alloy containing 3 wt.% of Al and 1 wt.% of Zn located in-between them were used as the ingoing materials (Fig. 1). They were cold-rolled before the EXW process. The ammonium nitrate mixed with fuel oil (ANFO), situated on the top of the set-up, providing appropriate detonation velocity was applied as the explosive material. The explosion was realized in air conditions, using parallel scheme. The initial thicknesses of A1050 (flyer plate), AZ31 (flyer plate) and A1050 (base plate) sheets were: 3 mm, 20 mm and 3 mm, respectively. They were later hot-rolled to the final thicknesses showed in Fig. 1. The samples for further investigations (5 mm × 10 mm × 2.6 mm) were cut from the central part of the clad. Annealing experiments were conducted in quartz ampoules (under vacuum conditions obtained with the use of a rotary pump) up to 10 h at the following temperatures: 300 °C, 350 °C and 400 °C. After a specified annealing time, the samples were cooled down in the ampoules to the room temperature.

The cross-section surface preparations for microstructural observations included grinding (P1000, P3000 and P5000) and polishing (0.25 μm diamond paste). Samples were washed with methanol and their contact with water was strongly avoided.

The surface observations were carried out using two scanning electron microscopes: FEI Quanta 3D FEG equipped with Trident energy dispersive X-ray spectrometer produced by EDAX and PHILIPS XL30 equipped with LINK ISIS EDS system (Oxford Instrument). The standardless analyses were performed at accelerating voltages of 10 kV, working distance of 10.0 mm in backscattered electrons (BSE) mode.

The width of the intermetallic phases layers were measured using a specialized computer program described in previous studies [23,24].

The thin foils were obtained from selected regions from the upper interface and prepared by the focused ion beam (FEI Quanta 3D Dual Beam Focused Ion Beam (FIB) instrument) technique. These specimens were subsequently used for TEM observations (FEI TECNAI G2 FEG super TWIN equipped with Phoenix EDS manufactured by EDAX) under an acceleration voltage of 200 kV.

In order to investigate the phase composition of the separated interfaces (see orange line in Fig. 1b), the diffraction of high-energy synchrotron radiation (87.1 keV, λ = 0.142342 Å) using beamline P07 at DESY in Hamburg, was applied.

Moreover, selected samples were analyzed using FEI Quanta 3D FEG equipped with the TSL EBSD system. Electropolishing was performed with the use of Struers electropolishing machine LectroPol-5 for 10 s with an electrolyte Struers AC2 using flow rate and voltage of 10 and 35-38 V, respectively. The temperature of electrolyte and the samples was 10 °C and 19 °C, respectively. Finally, the samples were cleaned with methanol. The EBSD measurement parameters were set to: the working distance of 10.0 mm, the tilt angle of 70°, the voltage of 20 kV and the mapping step size of 0.2 μm. The plane of observation was

perpendicular to the transverse direction (TD). The orientation of the single grains was obtained using inverse pole figure (IPF) color codding.

The hardness measurements were carried out on the cross-sectioned polished EXW samples before and after 4 hour- annealing at 400 °C. A microhardness tester CSM Instruments with a Vickers indenter was used at room temperature. The maximum applied load and dwell time of 0.09807 N and 15 s were used, respectively. The obtained results were averaged over 5 indentations.

The nanohardness tests were performed within the intermetallics areas by a nanohardness tester CSM Instruments at room temperature, using Berkovich indenter. The following parameters were used: the maximum applied load of 50 mN, the loading and unloading rate of 100 mN/min and the pause of 10 s. The results were also averaged over 5 individual indentations.

Fig. 1c summarizes the performed measurements with respect to the localization in the sample.

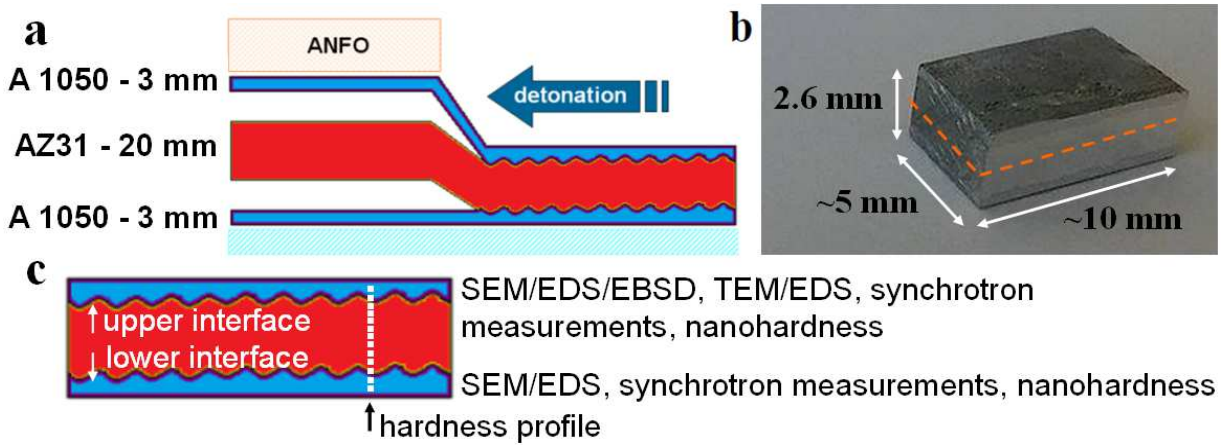

Fig. 1. (a) Schematic set-up of the explosively welded A1050/AZ31/A1050, (b) the specimen used in the experiments and (c) localization of performed experiments.

3. Results and discussion

3.1. Microstructure and phase composition of A1050/AZ31/A1050 samples after explosive welding

The SEM and TEM microstructure observations of the explosively welded and rolled samples by were performed as a first step of examination. The attention was paid to both the interfaces between the joined alloys and the type of formed intermetallic phases as well as to the structure of A1050 and AZ31 revealed by means of EBSD technique. Additionally, the phase composition was also confirmed using synchrotron radiation. Finally, all those data were referred to the hardness profile changes across the connection completed with the nanohardness values of the intermetallics.

Fig. 2 presents an interfacial microstructure of the A1050/AZ31/A1050 sandwich. Both upper and lower interfaces (Fig. 2a,b) had a wavy morphology with various humps amplitude (up to about 300 μm). A wavy-shaped interface is typical for the EXW method and was recognized previously for various joined pairs of metals or alloys: Zr700/carbon steel [27], Incoloy800/stainless steel 304 [28], aluminum (Al-1100)/copper (C-10100) [29] or A1050/AA2519 [30]. The oxides and impurities covering the parent clads were not observed at the interfaces areas, confirming the presence of the jetting phenomenon [31,32].

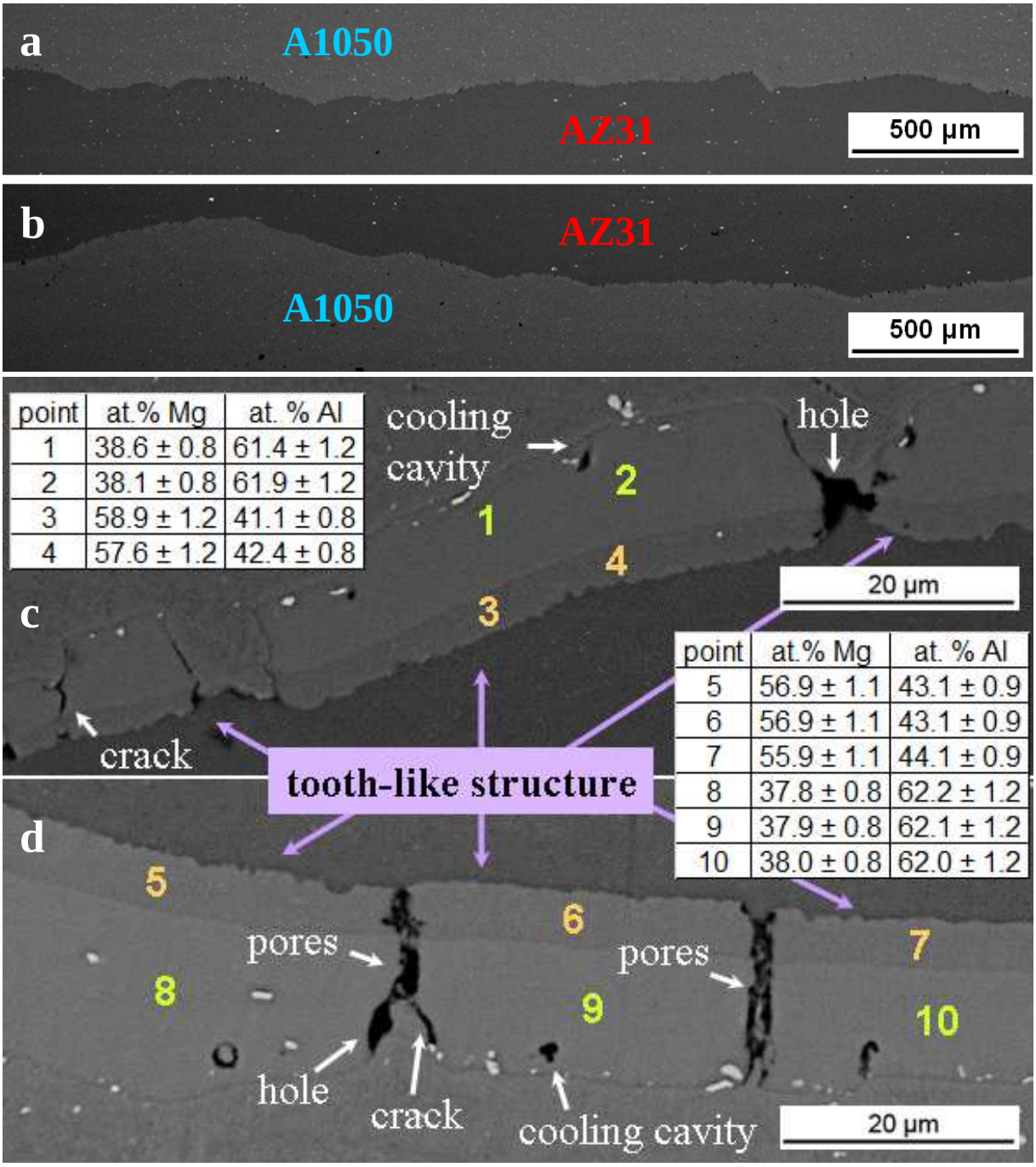

point	at.% Mg	at. % Al
1	38.6 ± 0.8	61.4 ± 1.2
2	38.1 ± 0.8	61.9 ± 1.2
3	58.9 ± 1.2	41.1 ± 0.8
4	57.6 ± 1.2	42.4 ± 0.8

point	at.% Mg	at. % Al
5	56.9 ± 1.1	43.1 ± 0.9
6	56.9 ± 1.1	43.1 ± 0.9
7	55.9 ± 1.1	44.1 ± 0.9
8	37.8 ± 0.8	62.2 ± 1.2
9	37.9 ± 0.8	62.1 ± 1.2
10	38.0 ± 0.8	62.0 ± 1.2

Fig. 2. SEM/BSE images of (a,c) the upper and (b,d) lower interface of A1050/AZ31/A1050 in the state directly after EXW with the corresponding EDS analysis.

Melted zones, forming tooth-like structures composed of two sub-layers, were evenly distributed at both interfaces (Fig. 2c,d). Inside those segments of various thicknesses, the presence of Mg_2Al_3 and $Mg_{17}Al_{12}$ was revealed by means of the SEM/EDS. Furthermore, pores, holes, cracks and cooling cavities were also observed, however they did not cause the interface delamination. The melted zones resulted from the initial melting during hot-rolling performed after explosive welding. The obtained microstructure was similar to that reported by Nie et al. in four-pass rolling combined with annealing experiments [11]. However, it was significantly different from the interfaces obtained by the EXW method and described in [13-20]. In the work of Ghaderi et al. [16], the only work, in which the intermetallics were observed in the state after EXW, the Al_2Mg phase formed locally in swirled areas. The difference in the phase composition of the intermetallic phases located at the interface might

arise due to both, different composition of aluminum alloy (A1050 in the present paper vs. A1100 in [16]) as well as various welding parameters (stand-off distance and detonation velocity). High detonation velocities promote the intermediate phase development through the formation of humps of high amplitude and great wavelength [16,33]. Moreover, many white dots irregularly distributed within the AZ31, A1050 clads and the intermetallic segments (mainly in Mg_2Al_3) could be distinguished in Fig. 2c,d. Unfortunately, they could not be properly studied by means of SEM/EDS due to their small size.

As a next step of the microstructure examination, the thin foils consisting of two intermediate sub-layers were cut from the upper interface with the FIB technique for the TEM analysis (Fig. 3). The TEM/EDS line scans, across the whole interface, allowed detecting the presence of two phases (Fig. 3a). The selected area diffraction patterns (SADPs) in Figs. 3e-g taken from the single grain of the intermetallic phase located closer to A1050 and to AZ31, confirmed the incidence of Mg_2Al_3 and $Mg_{17}Al_{12}$, respectively. Furthermore, TEM examination of Mg_2Al_3 phase evidenced its dual morphology: grains next to the A1050 clad were equiaxed, while going towards the AZ31 part, the grain shape changed to columnar (Figs. 3b,c,e and f). On the other hand, the $Mg_{17}Al_{12}$ intermetallic phase consisted of only one row of columnar grains (Figs. 3d and g).

A fine microstructure is typical for the EXW products, while large plastic deformation was obtained in various set-ups, for example steel/Zr 700 [34], A1050/Ti gr. 2 [23] or Ti gr. 2/low alloy steel st52-3N [35]. On the other hand, the columnar microstructure is rather unusual and was observed only in one case, of bimetallic 2205 stainless steel/X65 pipe steel [36]. However, the occurrence of fine and equiaxed grains, the same as in the present manuscript, was seen. The columnar grain shape is correlated with the direction of heat dissipation during the EXW process.

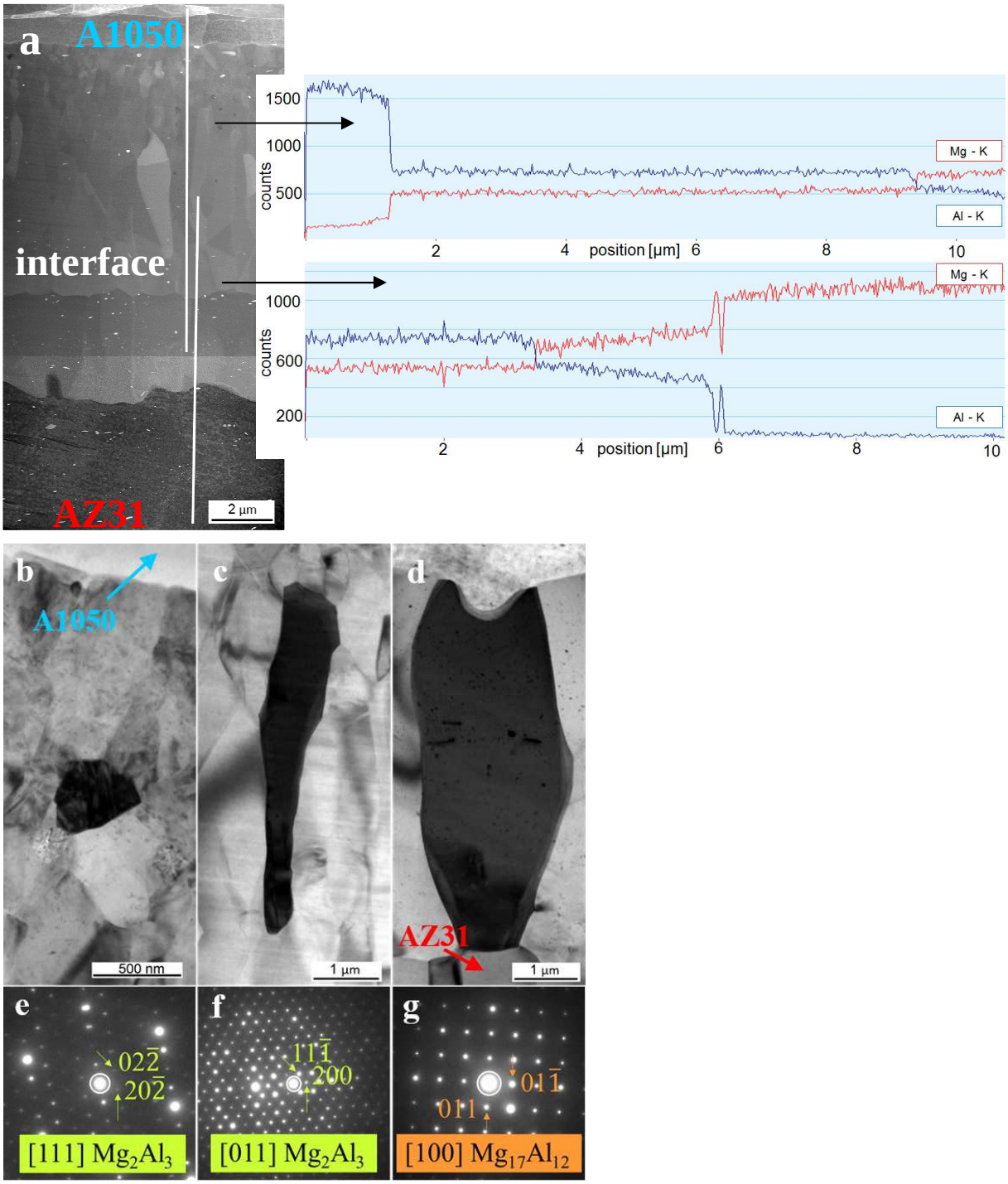

Fig. 3. (a) Scanning transmission electron microscopy image of the interface region with EDS line-scans demonstrating the changes in the chemical composition and (b,c,d) BF images of single grains together with (e,f,g) the corresponding SADPs.

Moreover, TEM/EDS point analyses of white dots (Fig. 4), noticed previously with SEM, demonstrate the presence of Al, Mg and Mn elements. Other detected elements originally do not come from the foil. Gallium comes from the FIB sample milling with gallium ions, copper from the grid, on which the FIB lamella was mounted.

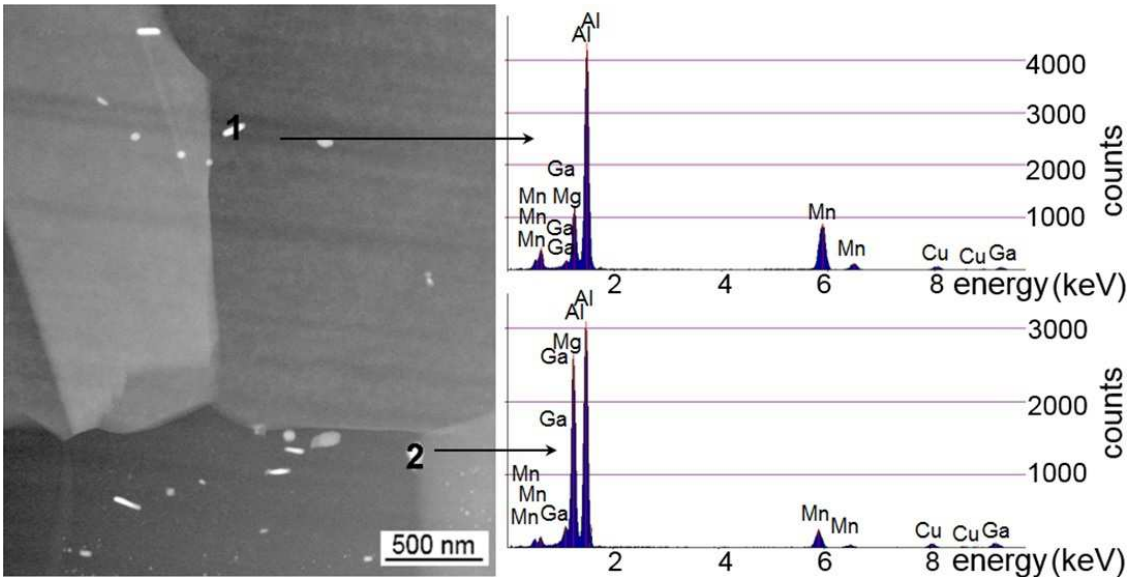

Fig. 4. Scanning transmission electron microscopy image of bright contrast precipitates with corresponding EDS point analysis.

The phase composition detected by SEM/TEM measurements was confronted with the results obtained by a monochromatic synchrotron X-ray beam studies (Fig. 5). The analysis of XRD pattern revealed that the most intense peaks come from Mg and Al. The interfaces were split for synchrotron studies before the analysis (see orange dashed-line in Fig. 1b), therefore small differences in the intensities of Mg reflections were registered for the upper and lower interface. A closer look to the weaker rings, through a change of intensity scale, allowed confirming three intermediate phases: Mg_2Al_3, $Mg_{17}Al_{12}$ and $Mg_{23}Al_{30}$ previously not detected with EDS. It was shown that both, lower (Fig. 5a) and upper (Fig. 5b) interfaces had the same phase composition.

The studies of the interface were supplemented by EBSD measurements taken from the upper interface, which provided information of the material microstructure after the EXW process (Fig. 6). Elongated grains of maximum length of about 450 µm and maximum width of about 100 µm were detected in the A1050 clad. It evidenced that the rolling after EXW, strongly influenced the clad microstructure. However, also the intensively refined structure in the close neighborhood of the bond, some small grains imprisoned between or within big grains or subgrain cross-patterns were noticed. On the other hand, a refined microstructure with decreasing grain size closer to the interface in AZ31 clad was observed. The refinement at interface region is a consequence of plastic deformation favored by the harsh conditions like extreme pressure, local high temperature and fast cooling during the EXW process. The average grain size, regarding AZ31 was determined to be 7.4 µm. Moreover, the volume fraction of the smallest ones (less than 10 µm) in AZ31 was 77.9%. Calculations of the misorientation angle distribution in both ingoing clads showed that the fraction of low angle grain boundaries (LAGBs), less than 15°, was equaled to 62.8% and 10.4% in A1050 and AZ31, respectively. Furthermore, two additional values of ~30° and ~86° were distinguished in AZ31. The former one is because of the {10-11}-{10-12} double twins and the recrystallization process where LAGBs are converted into high angle grain boundaries (HAGBs) [37], while the later one corresponds to the {10-12} tensile twinning which is easily triggered in Mg alloys [38].

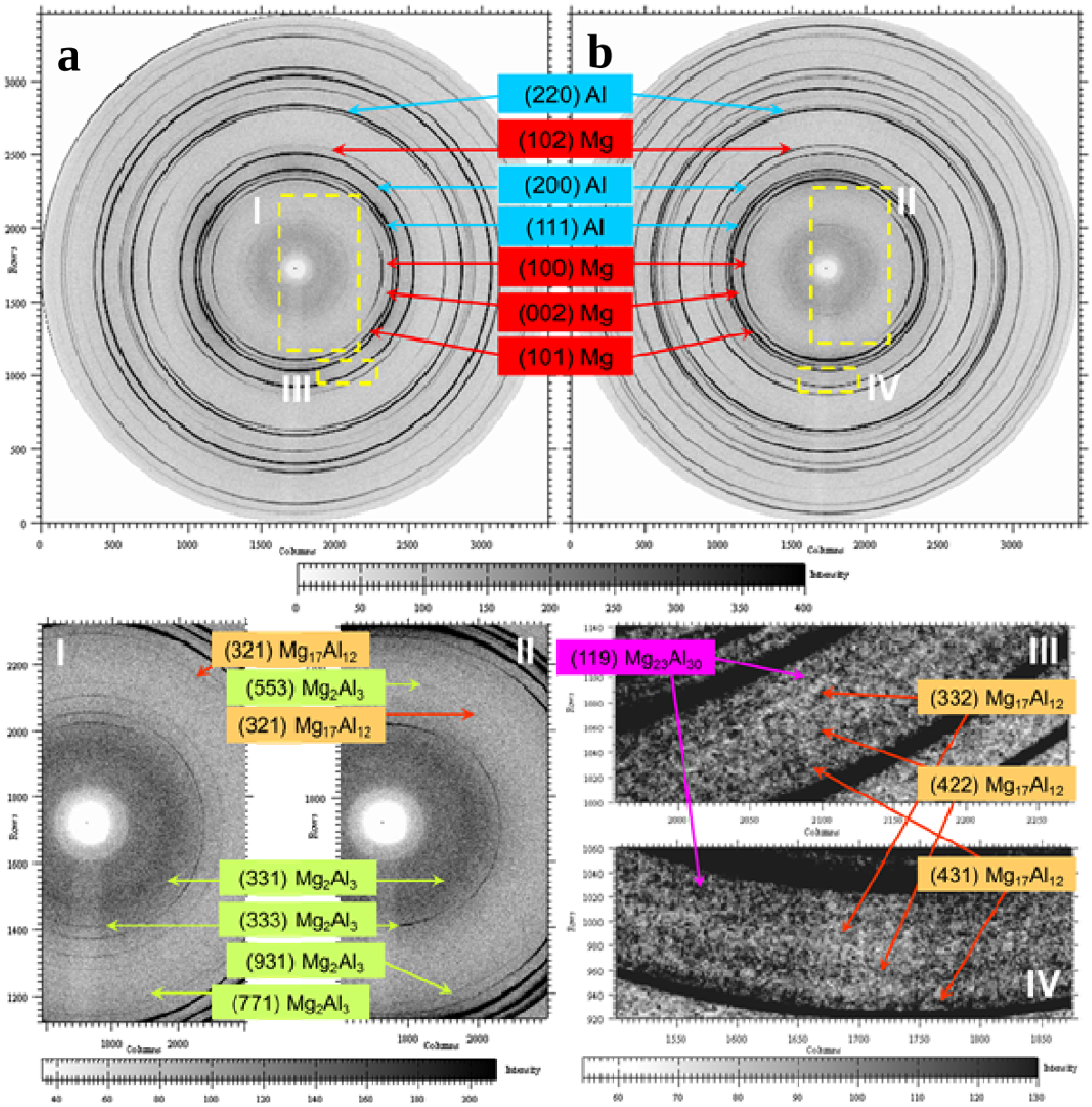

Fig. 5. Synchrotron analysis of (a) the lower and (b) upper interface of A1050/AZ31/A1050 in the state after EXW.

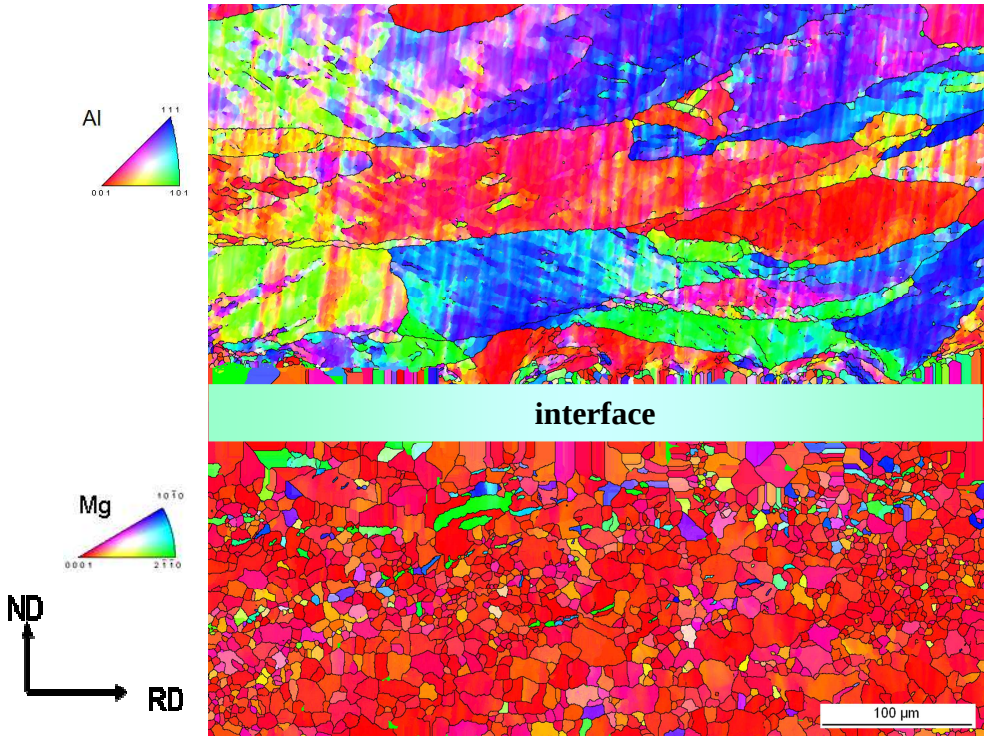

Fig. 6. SEM/EBSD map taken from the upper interface of A1050/AZ31/A1050 sample in the state after EXW. ND – normal direction, RD – rolling direction.

3.2. Microstructure and phase composition of A1050/AZ31/A1050 samples after annealing

The same research path as for the samples after explosive welding followed by rolling was applied for the characterization of the annealed A1050/AZ31/A1050 joints comprising of SEM/EDS, synchrotron radiation and EBSD in SEM.

The segmented structure at the interfaces strongly changed after heat treatment (Fig. 7). Annealing was performed in vacuum conditions at three temperatures of 300 °C, 350 °C and 400 °C selected based on the literature data [15]. It allowed obtaining continuous layers of intermetallic phases after 2 hours at each temperature. The SEM/EDS analysis gave similar results as in the state directly after EXW and the layer consisted of two sub-layers: Mg_2Al_3 and $Mg_{17}Al_{12}$. Moreover, the area, located adjacent to A1050 clad and Mg_2Al_3 intermetallic sub-layer, containing the intermetallic phase mixed with Mn precipitates significantly enlarged during each step of annealing experiment, regardless of the temperature used. Furthermore both upper and lower interfaces were similar for each temperature of heat treatment with respect to phase composition and its width (Fig. 8).

After annealing at the lowest temperature of 300 °C, the interfaces were of rather good quality, however randomly distributed voids, pores, cooling cavities or cracks could be observed. After 10 h of annealing, the presence of defects at the interface was observed very rarely (Fig. 7a), however, the intermetallics layer growth was the slowest comparing with 350 °C and 400 °C (Figs. 7,8).

After annealing at 350 °C, the microstructure was characterized by a good quality up to first 4 hours. After 6 h it changed significantly, due to the appearance of cracks through the Mg_2Al_3 phase. However, the crack propagation did not spread outside the Mg_2Al_3 phase. Furthermore, the third intermetallic phase, forming lenses randomly distributed in-between Mg_2Al_3 and $Mg_{17}Al_{12}$, was identified as $Mg_{23}Al_{30}$ by means of EDS analysis. The growth of this phase was pronounced only after heat treatment at 350 °C, which is consistent with the

equilibrium phase diagram [39], however, its discontinuous character remained even after 10 h (Fig. 7b).

At the highest temperature of annealing (400 °C), deterioration of the interface was detected after 10 hours. Again, it was manifested by the appearance of long and deep cracks through the Mg_2Al_3 intermetallic phase (Fig. 7c). The average value of the width of the Mg_2Al_3 and $Mg_{17}Al_{12}$ after 10 h of annealing was about 90 μm and 37 μm, respectively (Fig. 8).

Some cracks and other defects, such as holes and pores, were present across both interfaces in the state directly after EXW and rolling. They were formed at the borders among the tooth-like structure and ingoing materials, although they did not propagate across the intermetallic segments (Fig. 2). After annealing experiment for 10 h at 300 °C rather good quality of the interface composed mainly of two intermetallics (Mg_2Al_3 and $Mg_{17}Al_{12}$) forming sub-layers was obtained (Fig. 7a). The application of higher temperatures (350 °C and 400 °C) allowed manufacturing much wider layers, but characterized by much worse quality since the cracks run across the Mg_2Al_3 intermetallic phase (Figs. 7b,c).

The voids and pores are privileged places where cracking starts [40] through brittle intermetallics, characterized by low fracture toughness [41]. The interface analysis demonstrated that the precipitation hardening could be observed, as the area with Mn precipitates significantly expanded, creating a barrier for the crack propagation. On the other hand, some defects were observed within the Mg_2Al_3 phase close to the area with Mn precipitates. Also, the $Mg_{17}Al_{12}$ phase thermal coefficient is close to that of Mg, because of high concentration of Mg, therefore the conditions between Mg clad and $Mg_{17}Al_{12}$ are not conductive to stress formation. The Mg_2Al_3 and $Mg_{17}Al_{12}$ intermetallics, being the Al-rich and Mg-rich phases, respectively, have different thermal coefficients. Differences of thermal expansion between neighboring materials cause a tensile stress, leading to the crack formation [40], making the Mg_2Al_3 phase the weakest part of the interface. The crack propagation within Fe_xAl_y intermetallic phases, which formed the coating on boron steel was analyzed in the work of Zhong-Xiang et al. [40]. It was proved that differentiated thermal coefficient of each layer in composites can contribute to stress generation and crack propagation [40].

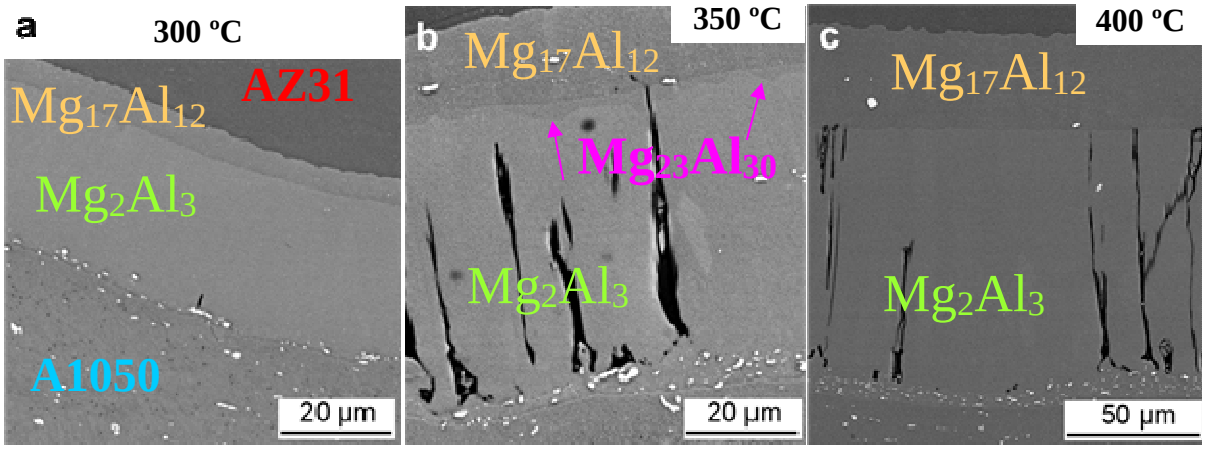

Fig. 7. SEM/BSE images of the lower interface of A1050/AZ31/A1050 in the state after annealing in vacuum conditions for 10 h, at (a) 300 °C, (b) 350 °C and (c) 400 °C, respectively.

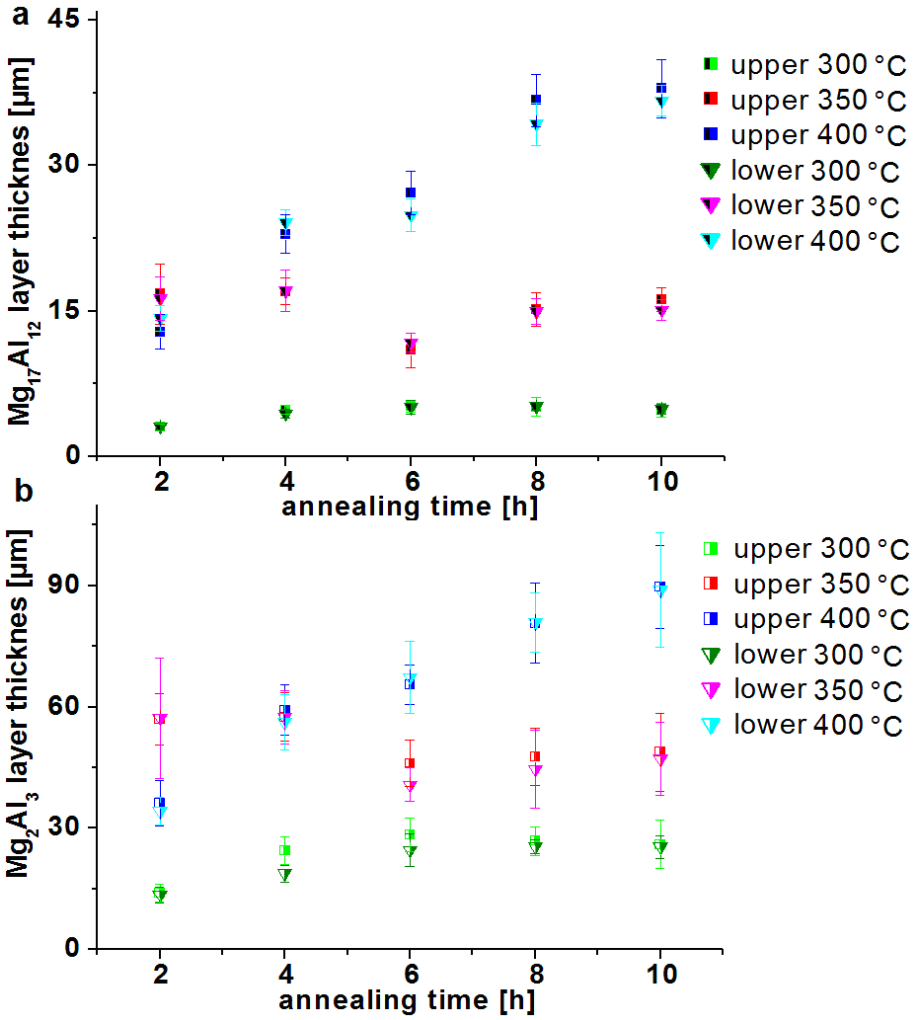

Fig. 8. Changes in the average width of the (a) $Mg_{17}Al_{12}$ and (b) Al_2Mg_3 intermetallic layers after annealing at three temperatures: 300 °C, 350°C and 400 °C with respect to the location of the interface in the sample.

Phase identification by synchrotron radiation measurements was also performed in the state after annealing for 10 h at 300 °C, 350 °C and 400 °C (Fig. 9). As in the case of not annealed material, Al and Mg reflections were characterized by the highest intensities. Comparison of the X-ray diffraction patterns for the lowest (300 °C) and the highest temperature (400 °C) showed a high similarity of the plots. The only difference was lower intensities of the intermetallics at 300 °C. Small amounts of $Mg_{23}Al_{30}$ were detected in both temperatures (Fig. 9), despite the SEM studies, which did not suggest its presence (Figs. 7a,c). It was indicated by the $Mg_{23}Al_{30}$ peaks, which did not overlap with other peaks (for example see peak (128)). However, many reflections belonging to $Mg_{23}Al_{30}$ overlapped with Mg_2Al_3 or $Mg_{17}Al_{12}$ peaks, increasing their intensities.

Moreover, a good agreement between SEM data and synchrotron measurement results was obtained for 350 °C. All three intermetallics: Mg_2Al_3, $Mg_{17}Al_{12}$ and $Mg_{23}Al_{30}$ detected in the state after EXW, were observed at the interfaces and there was no difference between upper (Figs. 7b,9) and lower interface, regarding to the intermediate phase composition.

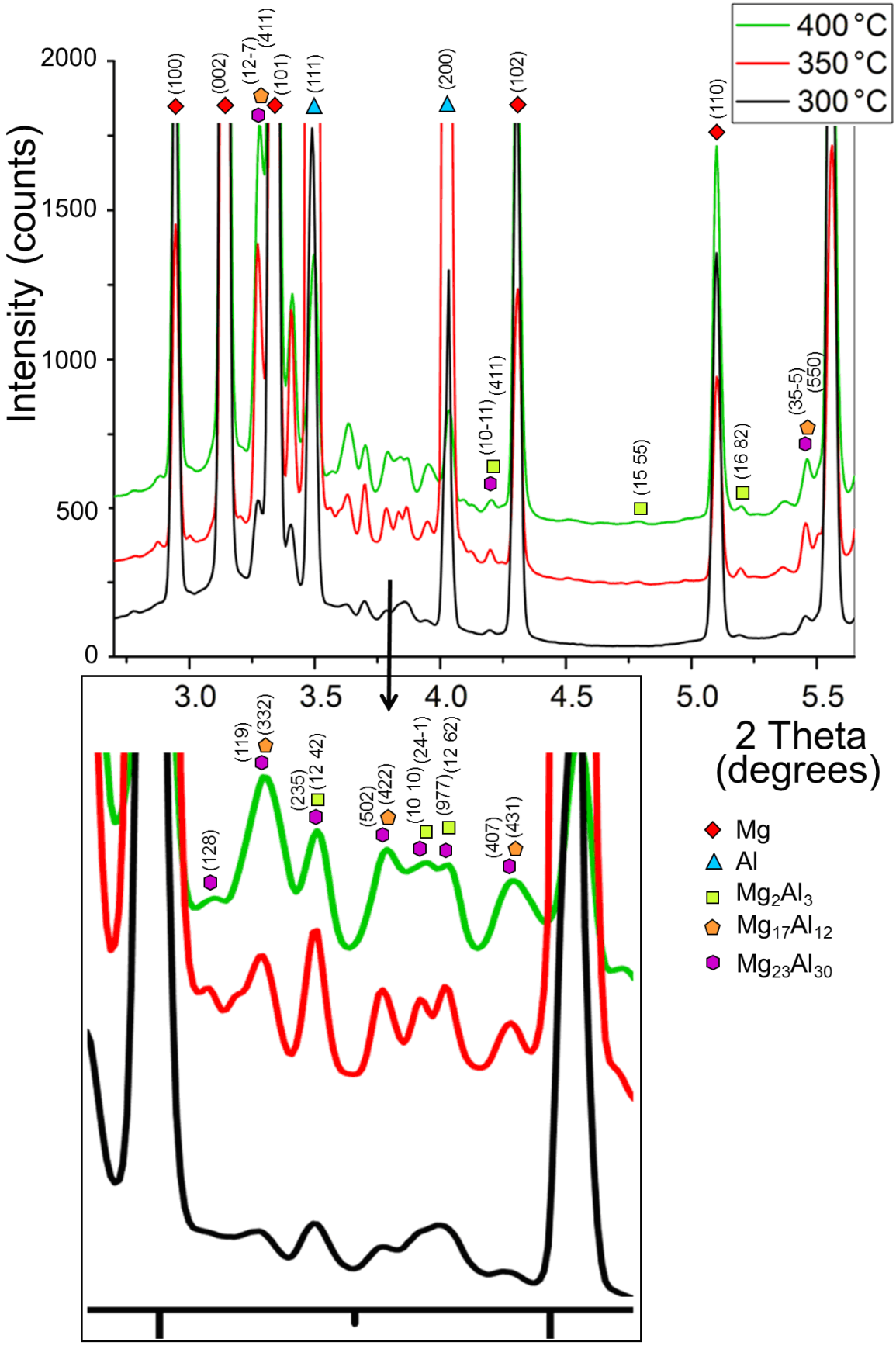

Fig. 9. The intermetallic phases composition changes at the upper interface of A1010/AZ31/A1050 explosively welded clads induced by heat treatment.

The SEM/EBSD measurements carried out for the sample after annealing for 10 h at 400 °C, are presented in Fig. 10a. The size and shape of both Mg and Al grains changed significantly as the result of the annealing process. An abnormal grain growth took place and the average grain size of Mg and Al was equaled to 14.1 μm and 56.2 μm, respectively (Figs. 10a). Fine microstructure was typical for Mg. On the other hand, some selected Al grains maintained elongated shapes, however generally due to heat treatment; they were characterized by an irregular shape. Furthermore, only in the case of Mg, grains changed their orientation dramatically (from red to green/blue), while in the Al clad the microstructure was still demonstrating similar distribution (Figs. 6,10).

Calculations of the misorientation angle distribution of the AZ31 and A1050 clads showed that the fraction of LAGBs, significantly decreased reaching 10.8% and 3.8% in A1050 and AZ31, respectively. The annealing process gave rise to boundary migration from LAGBs to HAGBs so the elevated frequency of peaks in the range of 20°-60° were distinguished in both clads, however it was more pronounced in AZ31.

Moreover, Figs. 10b and c show the mapping of the Mg and Al elements at the same area as region presented in Fig. 10a. The uniform distributions of the elemental components can be observed clearly in each sub-layer. Due to the fact that the elemental concentration decreases with increasing black intensity, higher concentration of Mg element in Mg_2Al_3 than $Mg_{17}Al_{12}$ phase and inverse relationship for Al element was confirmed.

In the case of Mg_2Al_3, the calculation of average grain size was performed separately for columnar and equiaxed grains indicating an average length 42.2 μm and width 9.9 μm for columnar and average diameter of 2.5 μm for equiaxed crystallites (Fig. 10a). Moreover, the fraction of LAGBs was equal to 3.6% and 4.2% for columnar and equiaxed grains, respectively (Fig. 10a). Additionally, three peaks were distinguished at about 20°, 40° and 57°, regardless of the grain shape. On the other hand, $Mg_{17}Al_{12}$ phase could not be indexed manifesting a very fine structure (Fig. 10a).

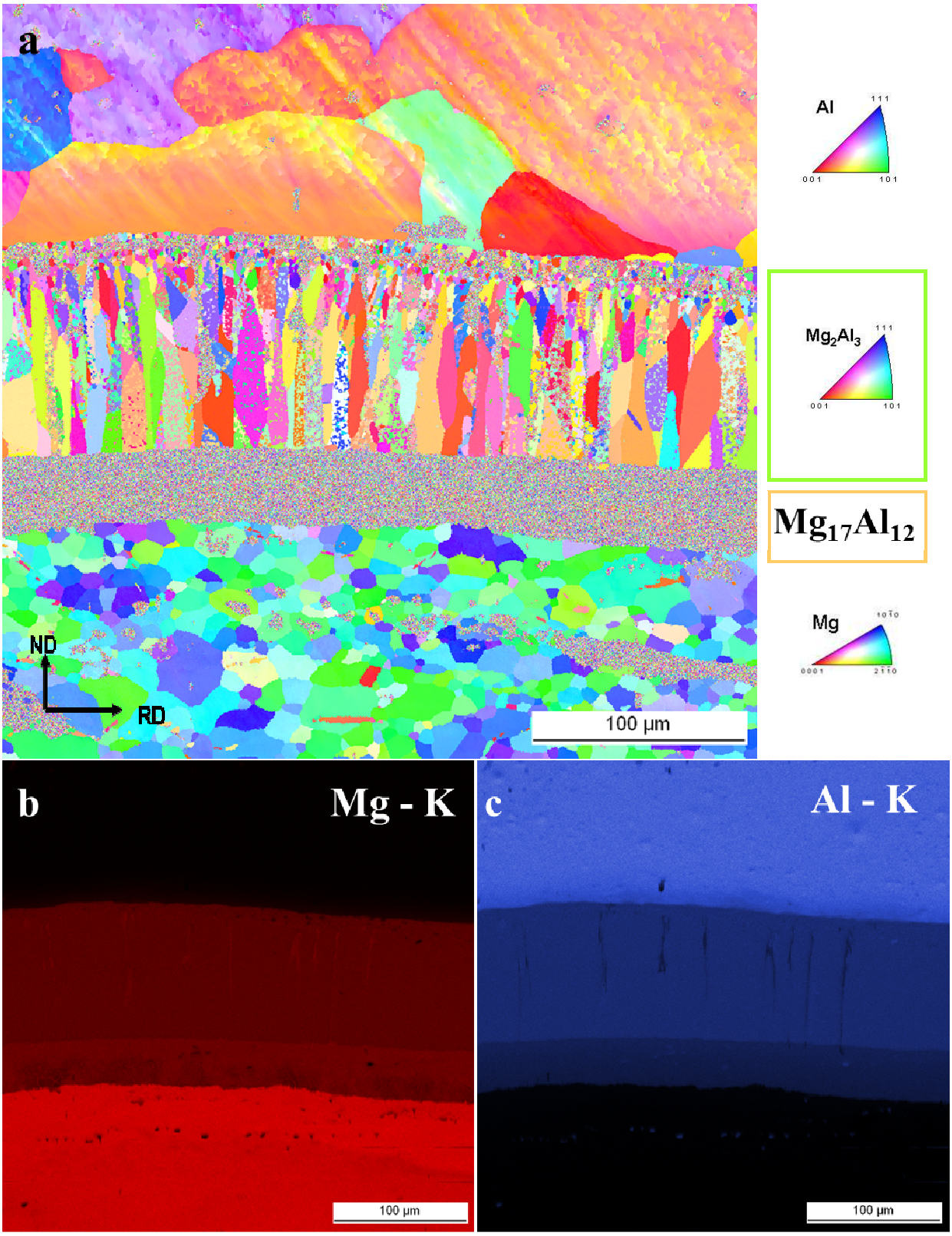

Fig. 10. (a) SEM/EBSD image of the upper A1050/AZ31/A1050 interface of the sample after annealing at 400 °C for 10 h in vacuum conditions with corresponding EDS maps analyses: (b) Mg-element and (c) Al-element.

3.3. Hardness and nanohardness measurements

The microstructure and phase composition results were accompanied with the hardness and nanohardness measurements. The average hardness of ingoing A1050 and AZ31 platters was equal to a value of about 34 HV and 80 HV, respectively.

Fig. 11 illustrates the hardness distribution across the entire A1050/AZ31/A1050 samples in both states: directly after EXW and after 6 h of annealing at 400 °C. The obtained hardness results were constant in the case of A1050 clad, regardless of whether it was upper (flyer) or lower (base) plate. The average values were within the range of 28 to 33 HV and 25 to 34 HV for A1050 after EXW and after subsequent annealing, respectively. It can be explained by the fact, that the mean grain size of aluminum alloy was large in the state before and after annealing and therefore, the observed changes are less pronounced. In contrary, AZ31 (flyer) clad was characterized by a large variation of hardness values in both analyzed cases before and after annealing. The average values varied in the range 49 - 62 HV and 52 - 63 HV for the state directly after EXW and after annealing, respectively. A large scatter of values for AZ31 was noticed due to the fine grained structure in comparison with A1050. In the case of AZ31 the annealing treatment changed the mean grain size from ~7 µm (before annealing) to ~14 µm (after annealing). However, it should be emphasized, that large scatter of the grain size within the AZ31 region can be also observed. This seems to be a reason of the hardness deviation shown in Fig. 11.

The analysis of nanohardness of the Mg_2Al_3 intermetallic phase was carried out for three cases: directly after EXW (when the tooth-like structure was present), after annealing for 6 h at 350 °C and for 6 h at 400 °C (when Mg_2Al_3 formed continuous layer). It was revealed, that the average nanohardness (HV) of Mg_2Al_3 equaled to 314.5 ± 14.6 HV and the Young modulus (E) was 62.0 ± 2.4 GPa after EXW and slightly changed into 328.9 ± 7.9 HV (E = 63.5 ± 1.0 GPa) and 347.0 ± 11.0 HV (E = 67.5 ± 1.5 GPa) after annealing at 350 °C and 400 °C, respectively. On the other hand, the nanohardness of the $Mg_{17}Al_{12}$ was measured only after heat treatment. It was established that the nanohardness of $Mg_{17}Al_{12}$ was similar to that of Mg_2Al_3, because it was 325.2 ± 4.4 HV (E = 67.2 ± 0.7 GPa) and 344.8 ± 6.7 HV (E = 75.1 ± 5.0 GPa) after annealing for 6 h at 350 °C and 400 °C, respectively.

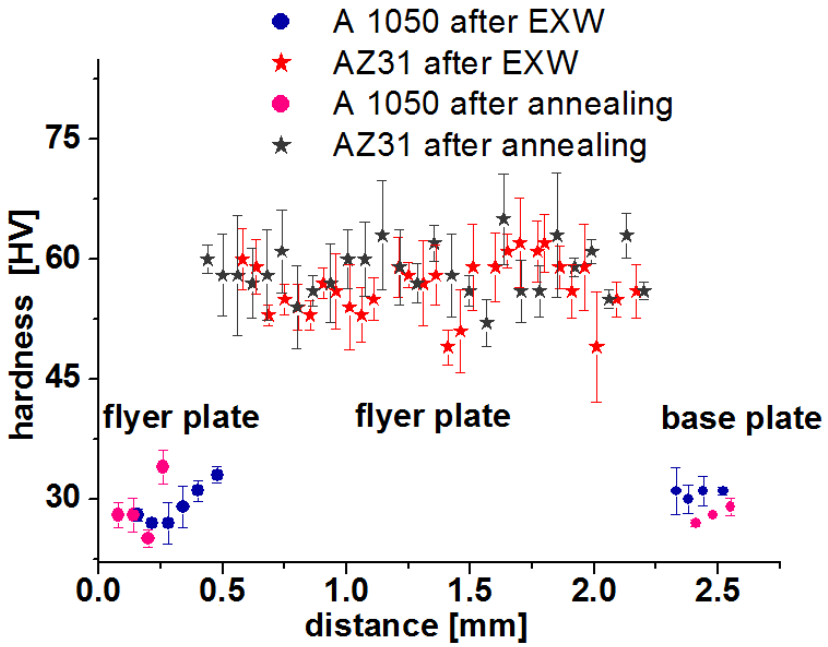

Fig. 11. Changes of hardness in A1050/AZ31/A1050 clads before and after annealing at 400 °C for 6 h in vacuum conditions.

3.4. Intermetallics growth kinetics calculations

For the description of the kinetics of intermetallics phase growth during annealing experiment, the formula $x = kt^n$, which correlates the average width of the layer (x) and time of annealing (t) was applied [42-45].

If the value of the *n* kinetic parameter is 1.0 or 0.5, then the mechanism of the intermetallics growth corresponds to the chemical reaction or the volume diffusion, respectively. When $n < 0.5$, one can expect some contribution of the grain boundary diffusion. Furthermore, the value of growth rate constant (*k*) determines how fast the phase growth proceeds in particular conditions [42,43].

The measured widths of each intermetallics were summarized in Fig. 8. The plot analysis related to 300 °C, showed that the plateau was achieved after 6 h of annealing. Therefore, only first three points were taken into consideration during growth kinetics calculation. The calculated values of *n* factor, obtained for upper interface after annealing at 300 °C, was found to be 0.51 and 0.66 for $Mg_{17}Al_{12}$ and Mg_2Al_3 , respectively. It means that the phases had different growth mechanisms: that of $Mg_{17}Al_{12}$ was controlled by the volume diffusion and that of Mg_2Al_3 was governed by mixed mechanism of the chemical reaction and the volume diffusion. The *n* values were similar for both intermetallics at lower interface, because it was equal to 0.48 and 0.54 for $Mg_{17}Al_{12}$ and Mg_2Al_3, respectively indicating that both phases growth was governed by the volume diffusion.

Interestingly enough, the intermetallics growth at both interfaces tends to be the zig-zag like at 350 °C. The decrease of the widths of $Mg_{17}Al_{12}$ and Mg_2Al_3 intermetallic phases, after 6 h of annealing, was correlated to their consumption by developing $Mg_{23}Al_{30}$ phase. Because of that, the calculations were not carried out for this temperature.

The calculations for 400 °C were performed for five time intervals. It was established that *n* factor, obtained for upper interface after annealing at 400 °C, was amounted to 0.69 and 0.55 for $Mg_{17}Al_{12}$ and Mg_2Al_3 , respectively. It confirmed that the mixed mechanism took place in both cases, however the contribution of the chemical reaction was smaller in the case of Mg_2Al_3 intermetallic phase. Again, there was no difference between phases at lower interface, since the *n* parameter was 0.58 and 0.59 for $Mg_{17}Al_{12}$ and Mg_2Al_3, respectively. It was clear that the growth was mainly controlled by the volume diffusion with some contribution of the chemical reaction. Moreover, some inhomogeneity in the exponential factor has been observed. For example, at 300 °C the n factor is quite different for the Mg_2Al_3 phase between upper and lower interface, as well as at 400 °C for the $Mg_{17}Al_{12}$ phase. These discrepancies can be explained by the influence of the localization of the interface with respect to the explosive material. Stronger grain refinement of the area in the close neighborhood of the interface was previously showed for another three-layered EXW system (A1050/Ti gr. 2/A1050) [42]. In that case, the closer to the explosion the more refined microstructure, the more contribution of reaction in the interface mechanism in the growth of the intermetallic phase. It can be presumed that the same situation takes place also in A1050/AZ31/A1050 clads, however this needs further studies.

Moreover, determination of the growth rate constant showed that $Mg_{17}Al_{12}$ intermediate phase grew slower than Mg_2Al_3 phase, regardless of the location in the sample. The *k* was 2.17 $\mu m/h^n$ and 9.12 $\mu m/h^n$ for $Mg_{17}Al_{12}$ and Mg_2Al_3, respectively for upper interface at 300 °C. These values were only slightly different for the lower interface, reaching the values of 2.27 $\mu m/h^n$ and 9.77 $\mu m/h^n$ for $Mg_{17}Al_{12}$ and Mg_2Al_3, respectively. Application of the higher temperature (400 °C) resulted in faster growth and the more pronounced difference in regard to the interface location. The *k* growth rate constant was 8.28 $\mu m/h^n$ and

25.25 μm/h^n for $Mg_{17}Al_{12}$ and Mg_2Al_3, respectively for upper interface and 9.80 μm/h^n and 23.49 μm/h^n for $Mg_{17}Al_{12}$ and Mg_2Al_3, respectively for lower interface. Calculated results of *n* factor and growth rate constant (*k*) were summarized in Table 1.

Obtained widths shown in the present work, were similar to those in the work of Zhang et al. [15] for experiments carried out at 300 °C and 400 °C. However, only the overall width of the continuous layer was measured, neither the width of each sub-layer was provided nor the kinetics calculations were carried out. Some discrepancies appeared in the case of 350 °C, however the annealing experiment was shorter involving only 4 h [15].

Table 1 Growth kinetics of $Mg_{17}Al_{12}$ and Mg_2Al_3 (comparison of upper and lower interface).

temperature of annealing	**300 °C**				**400 °C**			
calculation for	**upper interface**		**lower interface**		**upper interface**		**lower interface**	
intermetallic phase	**$Mg_{17}Al_{12}$**	**Mg_2Al_3**	**$Mg_{17}Al_{12}$**	**Mg_2Al_3**	**$Mg_{17}Al_{12}$**	**Mg_2Al_3**	**$Mg_{17}Al_{12}$**	**Mg_2Al_3**
exponential factor *n*	0.51	0.66	0.48	0.54	0.69	0.55	0.58	0.59
growth rate constant *k* *[μm/h^n]*	2.17	9.12	2.27	9.77	8.28	25.25	9.80	23.49
R^2	0.95	0.97	0.99	0.99	0.98	0.98	0.96	0.99
mechanism of growth	solely diffusion	mixed (chemical reaction + diffusion)	solely diffusion	solely diffusion	mixed (chemical reaction + diffusion)	mixed (mainly diffusion + chemical reaction)	mixed (mainly diffusion + chemical reaction)	mixed (mainly diffusion + chemical reaction)

4. Conclusions

It was established that, direct joining of three-layered A1050/AZ31/A1050 via EXW method can be performed. The investigation of the microstructure revealed satisfactory quality of interfaces. Intermediate phases formed tooth-like structures irregularly distributed along the interfaces. Each segment consisted of wider Mg_2Al_3 intermetallic phase, located closer to A1050 clad, thinner $Mg_{17}Al_{12}$, situated near to AZ31 clad and the minor amount of $Mg_{23}Al_{30}$.

Heat treatment experiments at 300 °C, 350 °C and 400 °C showed that the segmented structures transformed into continuous intermetallic layers, while the phase composition did not change. The quality of the interfaces was the best for the samples annealed at 300 °C. The layer of $Mg_{17}Al_{12}$ intermetallic phase and the zone with Mn precipitations acted as barrier to the propagation of cracks during annealing at higher temperatures.

The grain sizes and shapes were compared by analyzing EBSD maps in the states directly after EXW and after annealing at 400 °C. The magnesium alloy grains enlarged their size about twice. Typical microstructure of cold rolled materials was replaced by more equiaxed in A1050 clad.

Hardness measurements did not result in establishment of significant differences in A1050 and AZ31clads analyzed before and after annealing. Large scatter of hardness for AZ31 was noted and related to variation of the grain size. The nanohardness of Mg_2Al_3 and $Mg_{17}Al_{12}$ intermetallic phases was comparable and equaled to about 350 HV.

The growth kinetics calculations revealed the contribution of the “reaction at the interface” mechanism in growth of intermetallics for the upper interface, exposed for more drastic conditions during explosion. At 300 °C of annealing this contribution was observed for Mg_2Al_3 phase, while at 400 °C for $Mg_{17}Al_{12}$ intermetallic phase.

Acknowledgments

The authors express thanks to High Energy Technologies Works ‘Explomet’ (Opole, Poland) for the provision of A1050/AZ31/A1050 clads.

Samples were examined in the Accredited Testing Laboratories at the Institute of Metallurgy and Materials Science of the Polish Academy of Sciences in Cracow.

References

1. C. Liu, Y.Z. Zhang, L. Ye, High velocity impact responses of sandwich panels with metal fibre laminate skins and aluminium foam core, Int. J. Impact Eng. 100 (2017) 139–153 DOI: 10.1016/j.ijimpeng.2016.09.004
2. J. Godzimirski, J. Janiszewski, M. Roskowicz, Z. Surma, Ballistic resistance tests of multi-layer protective panels, Eksploat. Niezawodn. 17 (2015) 416–421 DOI: 10.17531/ein.2015.3.12
3. G.I. Kanel, S.V. Razorenov, A. Bogatch, A.V. Utkin, D.E. Grady, Simulation of spall fracture of aluminum and magnesium over a wide range of load duration and temperature, Int. J. Impact Eng. 20 (1997) 467–478 DOI: 10.1016/s0734-743x(97)87435-0
4. A. Manes, F. Serpellini, M. Pagani, M. Saponara, M. Giglio, Perforation and penetration of aluminium target plates by armour piercing bullets, Int. J. Impact Eng. 69 (2014) 39–54 DOI: 10.1016/j.ijimpeng.2014.02.010
5. A. Rohatgi, D.J. Harach, K.S. Vecchio, K.P. Harvey, Resistance-curve and fracture behavior of Ti–Al_3Ti metallic–intermetallic laminate (MIL) composites, Acta Mater. 51 (2003) 2933–2957 DOI: 10.1016/S1359-6454(03)00108-3
6. M. Konieczny, R. Mola, P. Thomas, M. Kopcial, Processing, microstructure and properties of laminated Ni-intermetallic composites synthesised using Ni sheets and Al foils, Arch. Metall. Mater. 56 (2011) 693–702 DOI: 10.2478/v10172-011-0076-y
7. N. Thiyaneshwaran, K. Sivaprasad, B. Ravisankar, Work hardening behavior of Ti/Al-based metal intermetallic laminates, Int. J. Adv. Manuf. Tech. (2016) DOI: 10.1007/s00170-016-9382-x
8. T. Tokunaga, K. Matsuura, M. Ohno, Superplastic behavior of Al-coated Mg alloy sheet, J. Alloys Compd. 601 (2014) 179-185 DOI: 10.1016/j.jallcom.2014.02.099
9. J.C. Liu, J. Hu, X.Y. Nie, H.X. Li, Q. Du, J.S. Zhang, L.Z. Zhuang, The interface bonding mechanism and related mechanical properties of Mg/Al compound materials fabricated by insert molding, Mater. Sci. Eng. A 635 (2015) 70–76 DOI: 10.1016/j.msea.2015.03.074
10. B. Zhu, W. Liang, X.R. Li, Interfacial microstructure, bonding strength and fracture of magnesium–aluminum laminated composite plates fabricated by direct hot pressing, Mater. Sci. Eng. A 528 (2011) 6584–6588 DOI: 10.1016/j.msea.2011.05.015
11. H. Nie, W. Liang, C. Chi, X. Li, H. Fan, F. Yang, Effect of annealing on microstructure and tensile properties of 5052/AZ31/5052 clad sheet, JOM 68 (2016) 1282–1292 DOI: 10.1007/s11837-015-1755-3

12. Yu.P. Trykov, V.G. Shmorgun, V.D. Rogozin, Yu.G. Dolgii, Technology of explosive welding magnesium-aluminium composite joints, Weld. Int. 17 (2003) 661–664 DOI: 10.1533/wint.2003.3186
13. Yu.P. Trykov, Y.G. Shmorgun, Y.N. Arisova, I.A. Ponomareva, The behavior of magnesium alloys during explosion welding and ways to prevent their failure, Russ. J. Non. Ferr. Met. 53 (2012) 139–144 DOI: 10.3103/S1067821212020149
14. V.N. Arisova, Yu.P. Trykov, O.V. Slautin, I.A. Ponomareva, A.E. Kondakov, Effect of heat treatment on mechanical properties and phase composition of magnesium-aluminum composite prepared by explosive welding, Met. Sci. Heat Treat. 57 (2015) 291–294 DOI: 10.1007/s11041-015-9877-3
15. N. Zhang, W. Wang, X. Cao, J. Wu, The effect of annealing on the interface microstructure and mechanical characteristics of AZ31B/AA6061 composite plates fabricated by explosive welding, Mater. Des. 65 (2015) 1100–1109 DOI: 10.1016/j.matdes.2014.08.025
16. S.H. Ghaderi, A. Mori, K. Hokamoto, Analysis of explosively welded aluminum-AZ31 magnesium alloy joints, Mater. Trans. 49 (2008) 1142–1147 DOI: 10.2320/matertrans.MC200796
17. Y.B. Yan, Z.W. Zhang, W. Shen, J.H. Wang, L.K. Zhang, B.A. Chin, Microstructure and properties of magnesium AZ31B–aluminum 7075 explosively welded composite plate, Mater. Sci. Eng. A 524 (2010) 2241–2245 DOI: 10.1016/j.msea.2009.12.007
18. P. Chen, J. Feng, Q. Zhou, E. An, J. Li, Y. Yuan, S. Ou, Investigation on the explosive welding of 1100 aluminum alloy and AZ31 magnesium alloy, J. Mater. Eng. Perform. 25 (2016) 2635–2641 DOI: 10.1007/s11665-016-2088-2
19. D. Balaga, D. Ostroushko, K. Saksl, E. Mazancova, O. Milkovic, Structure and mechanical properties of explosives welded Mg/A bimetal, Arch. Metall. Mater. 59 (2014) 1593–1597 DOI: 10.2478/amm-2014-0270
20. X. Yuan, W. Wang, X. Cao, T. Zhang, R. Xie, R. Liu, Numerical study on the interfacial behaviour of Mg/Al plate in explosive/impact welding, Sci. Eng. Compos. Mater. (2015) 1–10 DOI: 10.1515/secm-2015-0316
21. B. Gulenc, Investigation of interface properties and weldability of aluminum and copper plates by explosive welding method, Mater. Des. 29 (2008) 275–278 DOI: 10.1016/j.matdes.2006.11.001
22. F. Findik, Recent developments in explosive welding, Mater. Des. 32 (2011) 1081–1093 DOI: 10.1016/j.matdes.2010.10.017
23. D.M. Fronczek, R. Chulist, L. Litynska-Dobrzynska, Z. Szulc, P. Zieba, J. Wojewoda-Budka, Microstructure changes and phase growth occurring at the interface of the Al/Ti explosively welded and annealed joints, J. Mater. Eng. Perform. 25 (2016) 3211–3217 DOI: 10.1007/s11665-016-1978-7
24. D.M. Fronczek, J. Wojewoda-Budka, R. Chulist, A. Sypien, A. Korneva, Z. Szulc, N. Schell, P. Zieba, Structural properties of Ti/Al clads manufactured by explosive welding and annealing, Mater. Des. 91 (2016) 80–89 DOI: 10.1016/j.matdes.2015.11.087
25. J. Song, A. Kostka, M. Veehmayer, D. Raabe, Hierarchical microstructure of explosive joints: example of titanium to steel cladding, Mater. Sci. Eng. A 528 (2011) 2641–2647 DOI: 10.1016/j.msea.2010.11.092
26. H. Paul, L. Litynska-Dobrzynska, M. Prazmowski, Microstructure and phase constitution near the interface of explosively welded Aluminum/Copper plates, Metall. Mater. Trans. A 44 (2013) 3836–3851 DOI: 10.1007/s11661-013-1703-1

27. H. Paul, J. Morgiel, M. Faryna, M. Prazmowski, M. Miszczyk, Microstructure and interfacial reactions in the bonding zone of explosively welded Zr700 and carbon steel plates, Int. J. Mater. Res. 106 (2015) 782–792 DOI: 10.3139/146.111230
28. H. Zhao, P. Li, Y. Zhou, Z. Huang, H. Wang, Study on the technology of explosive welding Incoloy800-SS304, J. Mater. Eng. Perform. 20 (2011) 911–917 DOI: 10.1007/s11665-010-9712-3
29. M. Honarpisheh, M. Asemabadi, M. Sedighi, Investigation of annealing treatment on the interfacial properties of explosive-welded Al/Cu/Al multilayer. Mater. Des. 37 (2012) 122–127 DOI: 10.1016/j.matdes.2011.12.045
30. I. Szachogluchowicz, L. Sniezek, H. Sulym, M. Gloc, Testing and verification modeling of wave-shape formation under explosion welding to laminate AA 2519-Ti6Al4V, Proc. Struct. Integ. 2 (2016) 2375–2380 DOI: 10.1016/j.prostr.2016.06.297
31. J.G. Banker, E.G. Reinke: Explosion welding. ASM Handbook: Welding, Brazing and Solderig 6 (1993) 303–305
32. J. Song, A. Kostka, M. Veehmayer, D. Raabe, Hierarchical microstructure of explosive joints: example of titanium to steel cladding. Mater Sci Eng A 528 (2011) 2641–2647 DOI: 10.1016/j.msea.2010.11.092
33. M. Prazmowski, D. Rozumek, H. Paul, Influence of the microstructure on the fatigue cracks growth in the joint Zirconium-Steel made by explosive welding, SSP 258 (2017) 619–622 DOI: 10.4028/www.scientific.net/SSP.258.619
34. H. Paul, T. Baudin, F. Brisset, M. Prazmowski, Orientation changes near the interface of explosively bonded (carbon steel)/Zr700 sheets, IOP Conference Series: Mater. Sci. Eng. 82 (2015) 012056
35. M. Gloc, M. Wachowski, T. Plocinski, K.J. Kurzydlowski, Microstructural and microanalysis investigations of bond titanium grade1/low alloy steel st52-3N obtained by explosive welding. J. Alloy. Compd. 671 (2016) 446-451 DOI: 10.1016/j.jallcom.2016.02.120
36. L.J. Zhang, Q. Pei, J.X. Zhang, Z.Y. Bi, P.C. Li, Study on the microstructure and mechanical properties of explosive welded 2205/X65 bimetallic sheet. Mater. Des. 64 (2014) 462–476 DOI: 10.1016/j.matdes.2014.08.013
37. J.C. Tan, M.J. Tan, Dynamic continuous recrystallization characteristics in two stage deformation of Mg–3Al–1Zn alloy sheet, Mater. Sci. Eng. A 339 (2003) 124–132 DOI: 10.1016/S0921-5093(02)00096-5
38. Q. Jin, S.Y. Shim, S.G. Lim, Correlation of microstructural evolution and formation of basal texture in a coarse grained Mg–Al alloy during hot rolling, Scr. Mater. 55 (2006) 843–846 DOI: 10.1016/j.scriptamat.2006.05.040
39. T.B. Massalski, J.L. Murray, Binary Alloy Phase Diagram, ASM International USA, Ohio (1992)
40. G. Zhong-Xiang, W. Kai, Z. Yi-Sheng, Z. Bin, Cracking and interfacial debonding of the Al–Si coating in hot stamping of pre-coated boron steel, Appl. Surf. Sci. 316 (2014) 595–603 DOI: 10.1016/j.apsusc.2014.08.043
41. S. Kobayashi, T. Yakou, Control of intermetallic compound layers at interface between steel and aluminum by diffusion-treatment, Mater. Sci. Eng. A 338 (2002) 44–53 DOI: 10.1016/S0921-5093(02)00053-9
42. D.M. Fronczek, R. Chulist, Z. Szulc, J. Wojewoda-Budka, Growth kinetics of TiAl3 phase in annealed Al/Ti/Al explosively welded clads, Mater. Lett. 198 (2017) 160–163 DOI: 10.1016/j.matlet.2017.04.025
43. A. Wierzbicka-Miernik, K. Miernik, J. Wojewoda-Budka, K. Szyszkiewicz, R. Filipek, L. Litynska-Dobrzynska, A. Kodentsov, P. Zieba, Growth kinetics of the intermetallic phase in diffusion-soldered (Cu+5at.%Ni)/ Sn/ (Cu+5at.%Ni)

interconnections, Mater. Chem. Phys. 142 (2013) 682–685 DOI: 10.1016/j.matchemphys.2013.08.022
44. L. Xu, Y.Y. Cui, Y.L. Hao, R. Yang, Growth of intermetallic layer in multi-laminated Ti/Al diffusion couples, Mater. Sci. Eng. A 435 (2006) 638–647 DOI: 10.1016/j.msea.2006.07.077
45. W. Lee, K. Bang, S. Jung, Effects of intermetallic compound on the electrical and mechanical properties of friction welded Cu/Al bimetallic joints during annealing, J. Alloy. Compd. 390 (2005) 212–219 DOI: 10.1016/j.jallcom.2004.07.057